



Preparation and characterization of an solid oxide fuel cell tubular cell for direct use with sour gas



Adrien L. Vincent^a, Amir R. Hanifi^a, Mark Zazulak^a, Jing-Li Luo^{a,*}, Karl T. Chuang^a, Alan R. Sanger^a, Thomas Etsell^a, Partha Sarkar^{a,b}

^a Department of Chemical and Materials Engineering, University of Alberta, Edmonton, Alberta, Canada T6G 2G6

^b Environment & Carbon Management Division, Alberta Innovates – Technology Futures, Edmonton, Alberta, Canada T6N 1E4

HIGHLIGHTS

- The introduced cell is the first stackable metal-free membrane assembly for tubular solid oxide fuel cells.
- The cell is efficient for conversion of either sour gas or H₂S-containing hydrogen.
- The impregnation process allows construction of cathode supported SOFC membranes.
- H₂S promotes the hydrogen and the methane activation on LSBT.
- The obtained performances were comparable with industrial stacks.

ARTICLE INFO

Article history:

Received 29 October 2012

Received in revised form

7 March 2013

Accepted 19 March 2013

Available online 27 March 2013

Keywords:

SOFC
Microstructure
SrTiO₃
Impregnation
Perovskite

ABSTRACT

The first metal-free membrane assembly for tubular solid oxide fuel cells efficient in conversion of either sour gas or H₂S-containing hydrogen is fabricated and characterized. To achieve high performance, a porous layer of YSZ impregnated with LSBT, LSBT/YSZ (LSBT is La_{0.4}Sr_{0.5}Ba_{0.1}TiO₃), was selected as the composite anode material for the fully ceramic SOFC with the established catalyst LSM/YSZ as the cathode. The anode has a high performance and is stable in conversion of sulfur-containing fuels. The tubular fuel cell was characterized electrochemically using impedance spectroscopy (EIS) and potentiodynamic tests performed at 800, 850, and 900 °C with various fuels to determine the effect of H₂S content in the following feeds: H₂, H₂/H₂S (5000 ppm), and CH₄/H₂S (5000 ppm). Encouraging total power densities were obtained: 110, 105, and 41 mW cm^{−2}, respectively using H₂/H₂S, H₂, and dry CH₄/H₂S at 900 °C, despite high ohmic resistances.

© 2013 Elsevier B.V. All rights reserved.

1. Introduction

A major source of interest in solid oxide fuel cells (SOFCs) arises from their theoretical capability to use any oxidizable feed as fuel. Unfortunately, several prospective catalyst materials presently used in anodes are readily poisoned by one or more impurities such as H₂S or mercaptans, often present in unpurified anode feed gases [1–3]. Hence, the current generation of commercial SOFCs typically operates on highly purified hydrogen or highly purified methane, some expensive feeds, to ensure satisfactory performance and stability [4,5].

The majority of industrial H₂ is manufactured from hydrocarbon resources, often by steam reforming. The major anode catalyst poisons present in fuels derived from coal or lighter hydrocarbons are CO and H₂S. While it is possible to oxidize H₂S as fuel [6,7], the most efficient H₂ SOFC catalysts, notably Pt, Pd, and the cermet Ni/YSZ, react rapidly with H₂S either to form a sulfide or to poison the catalyst surface, even at low concentrations [8]. Therefore, one of the main challenges in development of new SOFCs is to enhance the stability of the anode in the presence of H₂S.

It has recently been shown [9–13] that LST and a doubly substituted strontium titanate (LSBT, La_{0.4}Sr_{0.5}Ba_{0.1}TiO₃) are promising anode materials in high H₂S content environments. Indeed, unlike Ni/YSZ, LST and LSBT are stable in a reducing atmosphere containing H₂S [14]. Moreover it was previously shown [13] that the addition of H₂S reduces the anode polarization resistance and dramatically increases the cell performance from

* Corresponding author. Tel.: +1 780 492 2232.

E-mail addresses: adrien.vincent@univ-tours.fr (A.L. Vincent), jingli.luo@ualberta.ca (J.-L. Luo).

2 mW cm⁻² in pure methane (inactive) to 450 mW cm⁻² with CH₄/H₂S 20% [13] which makes LST a preferred anode material.

Barium addition in LST (LSBT) significantly reduces the sintering temperature, which improves the anode performance without high sintering temperature.

Although tubular cells typically exhibit a lower power density than planar cells (due to their longer current paths), they are less prone to sealing problems and have better thermomechanical properties. Because of their excellent thermal shock resistance, the startup/shut down process is significantly faster than for planar fuel cells [15,16]. Different methods of ceramic processing, such as extrusion [17] and slip casting in combination with dip coating [17], have been effectively employed to produce tubular fuel cells. A thin, gas tight electrolyte on an anode supported cell enables achievement of higher power density compared to the corresponding electrolyte supported cells.

To produce tubular fuel cells, the impregnation processes described herein allow facile addition of electroactive materials throughout a porous matrix. Moreover, compared with mechanically mixing solids, the impregnation method enhances the ionic and/or the electronic pathway and the catalytic activity by the formation of interconnects between nano-sized particles [18,19].

The unit cell proposed in this work is a feasibility demonstration of the intermediate step between a laboratory cell and a stacked system. Given that our research objective is low cost power production directly from sour gases, low cell fabrication cost and H₂S resistance are our primary goal, superseding cell performance.

We will now describe the fabrication and characterization of the first metal-free membrane electrolyte assembly (MEA) for a cathode supported tubular cell, and use of a novel anode material for use with sour feeds.

2. Experimental procedures

2.1. Tubular matrix preparation

The tubular ceramic fuel cell used in this experiment consisted of a slip cast porous support approximately 400 μm thick which was converted to a cathode support following infiltration. The support was made using a mixture of calcined YSZ and 10 wt% NiO. Batista et al. [20,21] found that addition of small amounts of NiO to YSZ (8% of Yttrium) improves the sinterability of the electrolyte without affecting its overall conductivity. We similarly found that when 5–10 wt% NiO is incorporated into the slip cast porous support, a thinner gas tight electrolyte can be realized at 1350 °C compared with a NiO free support. Therefore, the porous support used for cathode infiltration was made utilizing calcined YSZ and a small amount of NiO. The tube upper inner diameter was about 6 mm, its bottom inner diameter was about 4.5 mm, and its length was about 7 cm. The top 1 cm of the tube was used as the sealing area to the gas impermeable support structure, and the active surface area of the fuel cell was 9.5 cm². The support was coated with a thin and dense YSZ electrolyte using the dip coating method. A thin and porous YSZ layer was coated onto the outer face of the tube, dried, calcined, and infiltrated with LSBT to form the anode. The porous support itself was infiltrated with LSM precursor solution to form the cathode.

2.1.1. Fabrication of the YSZ–NiO porous structure

To fabricate YSZ supports, YSZ powder (Tosoh TZ-8Y, 8 mol% Y₂O₃) first was calcined at 1500 °C for 3 h, cooled, and mixed with 10 wt% NiO (Baker 99+%) and water. The powder:water mass ratio was adjusted to 1:1 and the mixture was milled at 120 rpm for 72 h in a plastic bottle using 5 mm zirconia balls. The pH of the slip was set at 4.0 using 2% hydrochloric acid as the dispersant. To increase

the porosity of the support, 20 vol.% graphite (Sigma Aldrich <325 mesh) was added into the slip following pH adjustment, and the suspension was mixed for 15 min before slip casting. To create the tubular support, the slip was cast into a tubular plaster mold for 1 min after which the excess slip was poured out rapidly. The wet tube was then dried within the mold at room temperature. The resulting shrinkage facilitates its removal from the mold. The green tube was dried at 100 °C in an oven, heated at 700 °C for 1 h to oxidize graphite, then pre-sintered in air at 1150 °C for 3 h. Incorporation of the small amount of NiO increased the tube shrinkage, which reduced the incidence of electrolyte cracking during sintering. The final porous support porosity was 50 vol.%. Details of the methods used to fabricate thin, porous supports via slip casting are addressed elsewhere [22,23].

2.1.2. Coating with the dense YSZ electrolyte

The electrolyte suspension was prepared by mixing Tosoh YSZ, ethanol and binder (6 wt% ethylcellulose in terpineol). The slip was mixed for 1 h using zirconia balls, and then ultrasound was applied for 5 min to deaerate and disperse any agglomerated material. The slip was coated onto the pre-sintered porous support by dipping it into the suspension for 5 s and then dried. To ensure formation of a gas tight layer of electrolyte, the dip coating procedure was repeated 10 times. Following the final coating, the tube was dried and sintered at 1350 °C for 3 h to densify the electrolyte.

2.1.3. Creating the thin YSZ porous layer

To coat a thin porous layer for LSBT anode infiltration, YSZ (calcined at 1500 °C, milled for 72 h in water and dried) was mixed with 20 vol.% graphite, dispersant (Menhaden fish oil), azeotropic solvent (toluene/ethanol), and binder (polyvinyl butyral). The components were mixed at 300 rpm for 1 h in a planetary mill prior to coating. The mixture was applied to the electrolyte surface by briefly dip coating. The coated tube was heated to 300 °C then 700 °C in air for 1 h to burn off the organic components and graphite, it was next sintered at 1350 °C for 3 h. The final porosity of the thin porous layer was 50 vol.%.

Following testing, the samples were crushed and the fracture surfaces were analyzed using a JEOL 6301F field emission scanning electron microscope (FE-SEM). It was shown that calcination and milling of YSZ enabled control of its particle size and surface area and helped form a well-connected porous microstructure for fuel cell applications [24,25]. Torabi et al. [26] recently showed that the microstructure of the porous YSZ network significantly influences the surface area of the support, density of the triple phase boundary and, therefore, electrochemical performance of the LSM infiltrated cells. They found that using calcined YSZ produced a uniform, porous structure which provided the lowest ohmic resistance.

2.2. Anode catalyst layer preparation and impregnation

La_{0.4}Sr_{0.5}Ba_{0.1}TiO₃ (LSBT) was prepared within the porous YSZ matrix by precursor impregnation. The starting materials were lanthanum nitrate La(NO₃)₃·6H₂O (Alfa Aesar 99.9%), strontium nitrate Sr(NO₃)₂ (Sigma Aldrich), barium nitrate Ba(NO₃)₂ (Alfa Aesar 99+%) and titanium isopropoxide (Sigma Aldrich). The precursor solution contained citric acid (Alfa Aesar 99.5%), hydrogen peroxide in water (30%), ultra-pure water and Triton X-45. Nitrate precursors were dissolved in water to a total cation concentration of 2.5 × 10⁻³ mol L⁻¹. The titanium isopropoxide (TIP) reacted to form the peroxo-citrate in water by the addition of citric acid and hydrogen peroxide. The nitrate solution and the titanium peroxo-citrate solution were slowly mixed by vigorous stirring and produced a stable, deep red solution (no precipitates were detected after standing two months).

The anodic part of the tube was chosen to be the thin, porous, outer YSZ layer containing no NiO. This was because the porous support contained a small fraction of NiO, and it was necessary that there be no reaction of Ni in the presence of H_2S . The anode catalyst impregnations were performed with vacuum assistance; each impregnated layer was dried at 120°C and calcined at 800°C . The anode layer mass gain was 16.5% after five cycles. While this loading is lower than the usually required catalyst loading, it was the maximum obtained before structure obstruction and a drop in performance [27].

2.3. Cathode catalyst layer preparation and impregnation

Like the anode, the cathode was prepared by precursor impregnation. The solution used to infiltrate the cathode, LSM ($\text{La}_{0.85}\text{Sr}_{0.15}\text{MnO}_3$) was prepared by mixing appropriate amounts of $\text{La}(\text{NO}_3)_3 \cdot 6\text{H}_2\text{O}$ (Alfa Aesar), $\text{Mn}(\text{NO}_3)_2 \cdot \text{XH}_2\text{O}$ ($X \sim 5$) (Sigma Aldrich), $\text{Sr}(\text{NO}_3)_2$ (Sigma Aldrich), a small amount of Triton X-45 (Union Carbide Chemicals and Plastics Co. Inc.) and the minimum amount of water to dissolve all components when heated at 96°C resulting in a highly viscous, concentrated solution. The high viscosity solution was then impregnated into the porous support using a vacuum infiltration apparatus. The impregnated tube was dried in an oven at 150°C prior to heat treatment at 350°C to form the LSM phase. The total impregnated LSM was 6 wt% in the thick porous support layer.

2.4. Cell testing setup

The cell testing setup was assembled as shown in Fig. 1. Current collectors were formed on the inside surface of the tube from platinum ink and on the outside surface of the tube from gold ink. Wires were connected to the respective current collectors. Then the cell was sealed carefully onto its alumina tube support using a glass sealant (Ceramabond, Aremco Products). Nitrogen was slowly passed through the anode chamber as the cell was heated at a constant rate (5°C min^{-1}) to the selected operation temperature.

Methane containing 0.5% hydrogen sulfide ($\text{CH}_4/\text{H}_2\text{S}$), hydrogen (H_2) and hydrogen with 0.5% hydrogen sulfide ($\text{H}_2/\text{H}_2\text{S}$) were used as fuels and fed dry at a rate of 50 mL min^{-1} . Fuels were always supplied sequentially in the following order $\text{H}_2 \rightarrow \text{H}_2\text{--H}_2\text{S} \rightarrow \text{CH}_4\text{--H}_2\text{S}$. This sequence was used as it was found that it required a minimum time to reach an electrochemical equilibrium after each change of the feed, while the sequence had no effect on the

performance of the fuel cell using each fuel. Moreover, the observed phenomena were all reversible. Pure dry CH_4 was not tested as a fuel as previous tests on button cell showed that LSBT had very low activity for conversion of dry CH_4 [28].

Electrochemical properties were measured by potentiodynamic analyses at 10 mV s^{-1} . Results were saved after cycling the cell until a reproducible behavior was reached, using a Solartron instrument (SI 1287). Electrochemical Impedance Spectroscopy was done from $1 \times 10^5\text{ Hz}$ to $2.5 \times 10^{-2}\text{ Hz}$ after each power density measurement and always from a stable OCV.

A Rigaku Geigerflex X-ray diffractometer (XRD) system with a Co tube ($\lambda = 1.79026\text{ \AA}$) and a graphite monochromator was used to determine the purity of the crushed tube fragments. A Hitachi S-2700 Scanning Electron Microscope (SEM) was used to characterize cross sections of the tested tube.

3. Results and discussion

3.1. Impedance results

Fig. 2 shows a typical Nyquist curve obtained from a tubular cell test. The selected curve was obtained at 800°C with a sour gas feed. Frequencies mentioned on Fig. 2 are also representative of the obtained results showing their significantly low values and highlight the difficulty in accurately measuring concentration polarization. Three different area specific resistances can be dissociated in our system at high (ASR_Ω), medium (ASR_A) and low frequency phenomena (ASR_C). ASR_Ω , ASR_A et ASR_C are reported on the right part of Fig. 2 and provide the experimental results.

Considering ASR_Ω related to the “resistance” or to the “ohmic polarization”, the data shows only slight differences between the feed gases. ASR_Ω (ohmic losses) considers all the cell components including the thick cathode, interfaces, connections, wires etc. At 800°C the ASR_Ω trend is $\text{H}_2 < \text{H}_2/\text{H}_2\text{S} < \text{CH}_4/\text{H}_2\text{S}$. At 850°C the differences are reduced, with $\text{H}_2 < \text{H}_2/\text{H}_2\text{S} \approx \text{CH}_4/\text{H}_2\text{S}$, by 900°C all the ohmic resistances trend toward a similar value. As observed, ASR_Ω is slightly dependent on the feed gas. A possible reason for this is the reducibility of LSBT. Indeed, pure hydrogen is a strongly reducing gas in our temperature range and LSBT is conductive under reducing conditions. Additionally, uncracked methane is not as actively reducing as hydrogen, but as the temperature increases methane cracks and its reducing power strongly increases. The consequence is that LSBT is more easily reduced at 900°C than at 800°C and becomes more conductive at higher temperature.

Explaining the phenomenon related to ASR_A (A for activation) is a more delicate task and is assumed to be the charge transfer or activation polarization. ASR_A values are low and show some significant differences at 800°C which are in the same order as for ASR_Ω ($\text{H}_2 < \text{H}_2/\text{H}_2\text{S} < \text{CH}_4/\text{H}_2\text{S}$). Nevertheless, the differences exist mostly between the poisoned fuels and pure H_2 . An explanation could be that sulfur adsorbed on the anode surface, is in competition with oxygen as a possible species for anionic exchange, and increases the activation energy.

ASR_C (C stands for concentration) related to low frequency phenomena is ascribed to diffusion or concentration polarization. At 800°C no data are reported as the number of experimental “points” used to trace the Nyquist curve were too low to produce a meaningful fit, and performing the scans at a frequency lower than 0.25 Hz produced an unstable state. At 850°C and at 900°C the order for ASR_C , being $\text{CH}_4/\text{H}_2\text{S} < \text{H}_2/\text{H}_2\text{S} < \text{H}_2$, is the reverse of that observed in ASR_Ω or ASR_A . As previously observed and explained in-depth [13,27] sour gas always produced the best concentration resistance. Sour gas is a complex catalytic system and CH_4 with added H_2S results in some very active species on the anode surface (CS_2 and/or COS). Those species can be consumed if the cell is

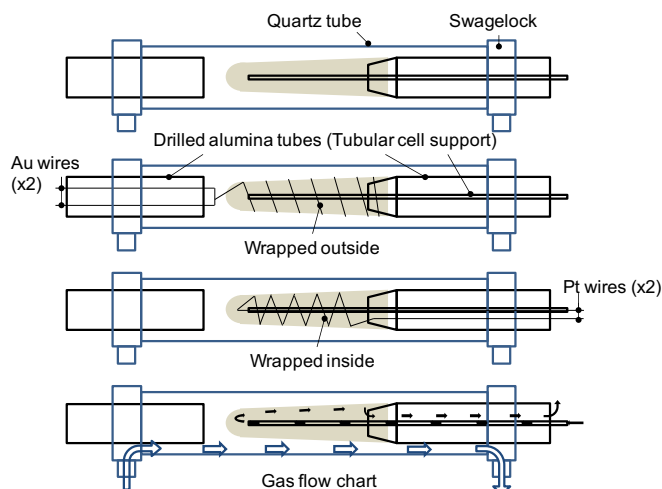


Fig. 1. Schematic figure of the testing setup.

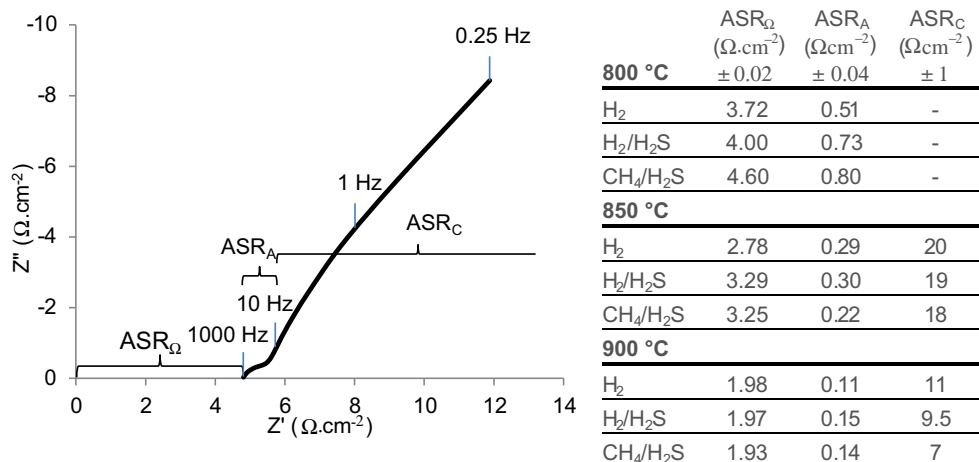


Fig. 2. Typical impedance spectrum and impedance data (Ω cm⁻²) for the tested tubular cell at 800, 850 and 900 °C for different feed gases.

running, but will quickly accumulate on the surface of the anode if it is not. This accumulation of active species causes a low ASR_C and is responsible for the initial segment of the IV curves which will be discussed in the following paragraph.

This phenomenon that occurs between CH₄ and H₂S is efficient and key to our system as it's highly resistant to H₂S corrosion or poisoning.

3.2. Electrical performance

I/V curves provide more insight than the single power density values alone. Fig. 3 shows the I/V curves obtained at 800, 850 and 900 °C for the three different feed gases using tubular cells having impregnated LSBT catalyst as anode.

Fig. 3a was obtained at 800 °C using pure H₂, H₂/H₂S and CH₄/H₂S fed sequentially. The maximum current density 84 mA cm⁻² and the maximum power density 63 mW cm⁻² were obtained with H₂/H₂S, followed by pure H₂ with 69 mA cm⁻² and 45 mW cm⁻² and finally by CH₄/H₂S with 20 mA cm⁻² and 14 mW cm⁻². The shapes of the CH₄/H₂S curves had three distinctive parts: a high voltage domain, wherein the I/V curve showed good performances, a medium range voltage where the performances are reasonable, and a low voltage domain wherein there was a sudden, strong decrease in current density. Previously observed [13], this overall behavior was attributable to a change in the methane electro-oxidation conversion mechanism. Between OCV and 1.05 V the cell consumes the highly active species (CS₂) which is chemically produced at the anode surface from CH₄ + H₂S. While this chemical process is faster than the fuel electro-oxidation, the cell performances are comparable with hydrogen. Between 1.05 V and 0.75 V the fuel electro-oxidation requires more fuel than what can be chemically produced, as a consequence, H₂S becomes the next active species and starts to be partially oxidized. However, partially oxidized sulfur is also a very active species and reacts readily with CH₄ to produce CO or CO₂ regenerating H₂S (this cycling phenomenon is the intrinsic definition of a catalyst). Below 0.75 V the activated sulfur begins to be fully oxidized to its stable state SO₂ and can no longer act as an activated species to transfer oxygen to carbon. The result is a sudden and progressive drop in the methane oxidation rate forcing a reduction in current evolution due to the catalyst destruction. Considering the OCV, it was 1.22 V in H₂, 1.24 V in H₂/H₂S, and 1.13 V in CH₄/H₂S, these high values show that the system did not leak and was sealed effectively by the glass sealant.

Fig. 3b was obtained at 850 °C using the same feeds. The performance order was the same as at 800 °C. However, the performance obtained with pure H₂ was closer to that of the H₂/H₂S mixture while the performance obtained with sour gas was still

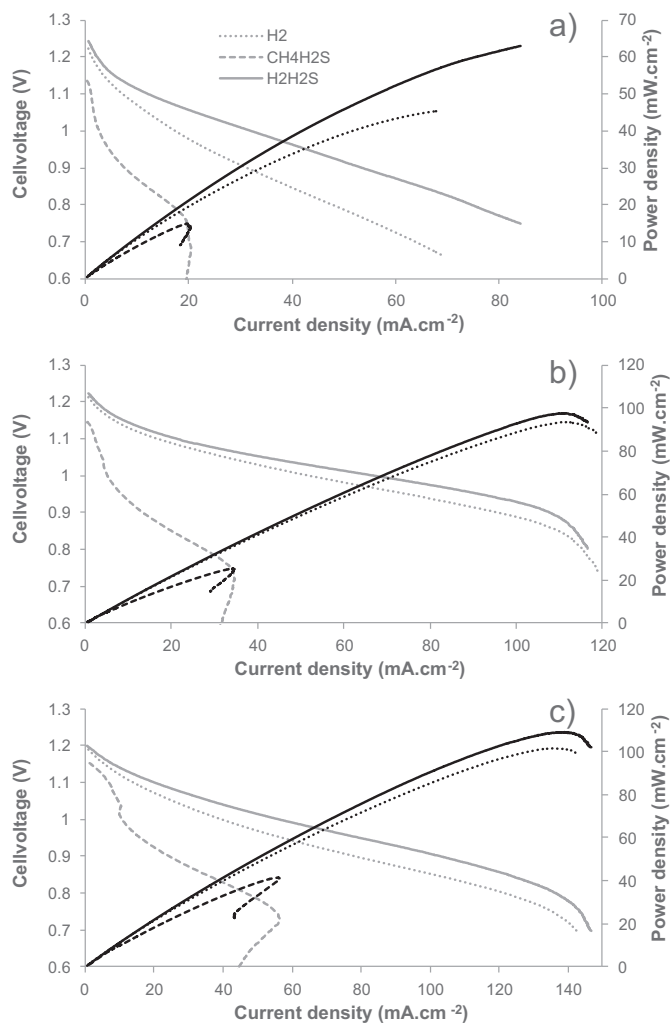


Fig. 3. Compensated IV curves obtained using H₂, CH₄H₂S (5000 ppm) and H₂H₂S (5000 ppm) at a) 800 °C; b) 850 °C; and c) 900 °C.

low. In addition, mass transfer blocking effects were observed at high current for $\text{H}_2/\text{H}_2\text{S}$ and pure H_2 . At 850°C the OCV was 1.21 V in H_2 , 1.22 V in $\text{H}_2/\text{H}_2\text{S}$, and 1.14 V in $\text{CH}_4/\text{H}_2\text{S}$, the same order as at 800°C . Fig. 3c shows the performance at 900°C again using H_2 , $\text{H}_2/\text{H}_2\text{S}$ and $\text{CH}_4/\text{H}_2\text{S}$ as feed fuels. The shapes of the curves at 900°C were very similar to those obtained at 850°C , and no new features were observed for these curves. Following the same trend seen at 800°C and 850°C , the OCV's were 1.19 V in H_2 , 1.20 V in $\text{H}_2/\text{H}_2\text{S}$, and 1.15 V in $\text{CH}_4/\text{H}_2\text{S}$. As expected, the performance was superior to that at lower temperatures and the cell produced 110 mW cm^{-2} when using $\text{H}_2/\text{H}_2\text{S}$ as fuel with a current density of 147 mA cm^{-2} . For comparison, Aguilar et al. [29] produced 90 mW cm^{-2} in $\text{H}_2\text{--H}_2\text{S}$ (5%) at 900°C with a button cell, showing the present tubular cell to be superior in performance.

However, a direct comparison of the present tubular cell with prior button cells is tenuous, since no button cell has been described having the same structure with the same materials. The results obtained using sour gas show that, even if the tube was active in $\text{CH}_4/\text{H}_2\text{S}$ oxidation, power production remains low. Nevertheless, these results are promising as the cell described herein has the first metal-free MEA for a tubular fuel cell, and achieved about half of the power density of an optimized conventional industrial stack. The cell is produced with H_2S -tolerant, low cost ceramic materials, and can be manufactured using low cost fabrication processes. As indicated in the previous section, the ohmic losses were an important feature of the cell as tested, and arise mainly from its cathode support configuration. The ohmic resistance introduces a dramatic loss of cell performance. A future development will be to test a similar tube in an anode supported configuration. Long term stability tests will determine whether LSBT can be considered for use in a durable, sulfur resistant fuel cell.

3.3. Microstructural analysis

3.3.1. SEM observations

Fig. 4 shows a cross section of the tube cell after testing. The two smaller illustrations show both electrodes at higher magnification. The left part of the figure is the porous YSZ support which was converted to the cathode ($430\text{ }\mu\text{m}$) then, from left to right, are the electrolyte ($40\text{ }\mu\text{m}$) and the porous YSZ converted to form the thin

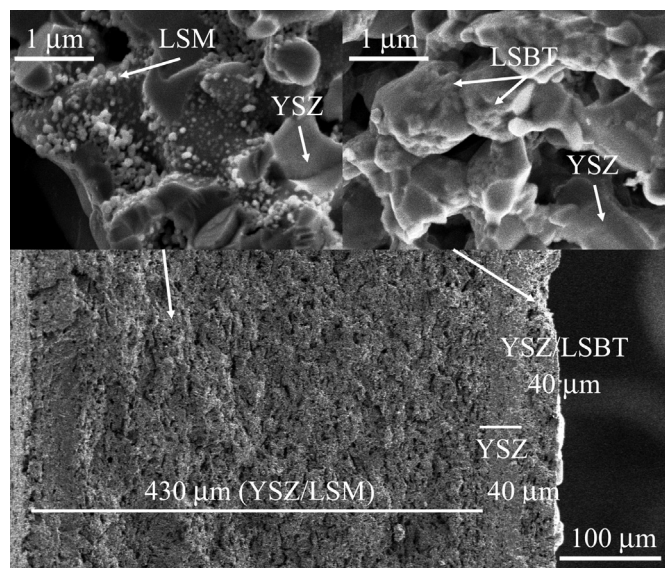


Fig. 4. SEM image of the tube cross section (bottom) and higher magnifications of LSM/YSZ (top left) and LSBT/YSZ (top right).

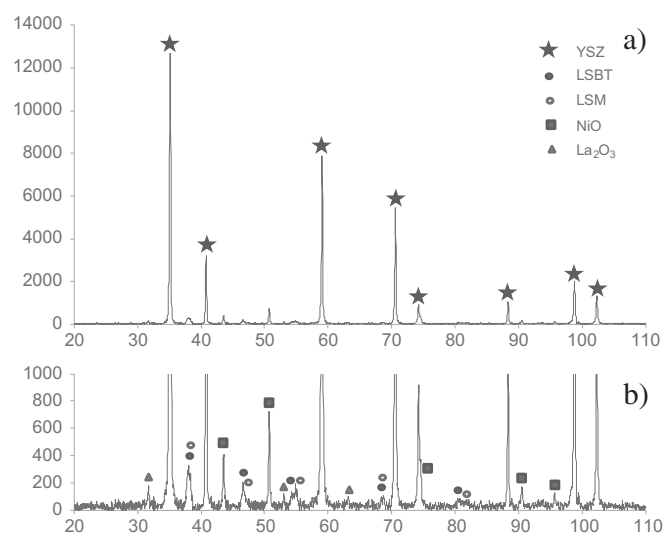


Fig. 5. a) Fully indexed XRD pattern obtained on a ground tube fragment after tests, and b) magnified scale of the same XRD pattern showing indexed lines for the minor phases.

anode layer ($40\text{ }\mu\text{m}$). The total thickness of the tube is about $500\text{ }\mu\text{m}$. The top left illustration shows the cathode at high magnification allowing observation of the LSM particles. In general, the LSM particle size was between 20 and 100 nm and well dispersed throughout the YSZ matrix, with a slightly higher content in the matrix depressions. From a global point of view, the LSM particles insured a high specific area as their nanometric size was stable. However, the observed particle dispersion throughout the thick YSZ matrix suggested one possible origin for the high ohmic resistances determined from the impedance measurements.

In the anode layer, the LSBT covering was high on YSZ, with particle sizes in the range of 100 nm . Unlike LSM, LSBT is a MIEC (mixed ionic electronic conductor) and the YSZ matrix was almost fully covered by LSBT to optimize performance.

Whether the cathode or the anode is the supporting layer, the present data show that properly impregnating the thick supporting layer is a key to good cell performance.

3.3.2. XRD analyses

To study the stability of the overall tube, XRD analyses were performed on ground fragments of the tube (Fig. 5). The main part of the figure is the complete pattern. As expected, YSZ was the major component, identified by stars in the top pattern. In the bottom spectrum the magnified vertical scale shows the detailed pattern which enabled identification of minor phases also present. As expected, indexed signals for LSBT, LSM and NiO were detected in addition to YSZ. As these components were present in small amounts, other peaks overlapped, and were not clearly identified. La_2O_3 may also have been present as a possible secondary phase derived from LSBT by lanthanum ex-solution from LSBT and/or LSM.

4. Conclusions

This is the first time that a metal-free membrane electrode assembly for tubular fuel cells has been constructed and shown to perform well with high H_2S -containing fuels. The YSZ matrix tubular cell had as an inside porous support layer, a thin electrolyte deposited thereon and a thin outer porous layer. Impregnating the inner porous layer with LSM to form the cathode and the outer layer with LSBT to form the anode completes fabrication of the tubular cell. Impedance tests were performed from 800 to 900°C

using H_2 , $\text{H}_2\text{--H}_2\text{S}$ and $\text{CH}_4\text{--H}_2\text{S}$ as fuels. The presence of H_2S decreased the ohmic resistance slightly, which was consistently high as a consequence of the electrolyte thickness. One possible further cause of the observed ohmic loss was lack of LSM in the cathode.

Power cell tests were performed under conditions similar to those for determination of impedance and, as expected, the performances were not impacted by the presence of H_2S but were even modestly improved when it was present. Measured OCVs were, respectively, 1.22, 1.21 and 1.15 V when using $\text{H}_2/\text{H}_2\text{S}$, H_2 and $\text{CH}_4/\text{H}_2\text{S}$ as feed at 850°C , and the corresponding maximum power densities were 109, 102 and 41 mW cm^{-2} , respectively, using $\text{H}_2/\text{H}_2\text{S}$, H_2 and dry $\text{CH}_4/\text{H}_2\text{S}$ at 900°C .

Acknowledgments

This research was supported through funding to the NSERC Solid Oxide Fuel Cell Canada Strategic Research Network from the Natural Science and Engineering Research Council (NSERC) and other sponsors listed at www.sofccanada.com.

References

- [1] M. Gong, X. Liu, J. Trembly, C. Johnson, *Journal of Power Sources* 168 (2007) 289.
- [2] M. Alifanti, R. Auer, J. Kirchnerova, F. Thyron, P. Grange, B. Delmon, *Applied Catalysis B: Environmental* 41 (2003) 71.
- [3] K. Haga, S. Adachi, Y. Shiratori, K. Itoh, K. Sasaki, *Solid State Ionics* 179 (2008) 1427.
- [4] J.P. Trembly, A.I. Marquez, T.R. Ohn, D.J. Bayless, *Journal of Power Sources* 158 (2006) 263.
- [5] Y. Matsuzaki, I. Yasuda, *Solid State Ionics* 132 (2000) 261.
- [6] A.A. Davydov, V.I. Marshneva, M.L. Shepotko, *Applied Catalysis A: General* 244 (2003) 93.
- [7] K.T. Chuang, J.-L. Luo, A.R. Sanger, *Chemical Industry and Chemical Engineering Quarterly/CICEQ* 14 (2008) 69.
- [8] J.F.B. Rasmussen, A. Hagen, *Journal of Power Sources* 191 (2009) 534.
- [9] D.P. Fagg, V.V. Kharton, A.V. Kovalevsky, A.P. Viskup, E.N. Naumovich, J.R. Frade, *Journal of the European Ceramic Society* 21 (2001) 1831.
- [10] X. Sun, S. Wang, Z. Wang, X. Ye, T. Wen, F. Huang, *Journal of Power Sources* 183 (2008) 114.
- [11] K. Ahn, S. Jung, J.M. Vohs, R.J. Gorte, *Ceramics International* 33 (2007) 1065.
- [12] X. Huang, H. Zhao, X. Li, W. Qiu, W. Wu, *Fuel Cells Bulletin* 2007 (2007) 12.
- [13] A.L. Vincent, J.-L. Luo, K.T. Chuang, A.R. Sanger, *Applied Catalysis B: Environmental* 106 (2011) 114.
- [14] R. Mukundan, E.L. Brosha, F.H. Garzon, *Electrochemical and Solid-State Letters* 7 (2004) A5.
- [15] K. Kendall, *International Journal of Applied Ceramic Technology* 7 (2010) 1.
- [16] K.S. Howe, G.J. Thompson, K. Kendall, *Journal of Power Sources* 196 (2011) 1677.
- [17] L. Zhang, J. Liu, J. Yin, *Journal of Fuel Cell Science and Technology* 7 (2010) 1.
- [18] T.Z. Sholklapper, C.P. Jacobson, S.J. Visco, L.C. De Jonghe, *Fuel Cells* 8 (2008) 303.
- [19] J. San Ping, *Materials Science and Engineering: A* 418 (2006) 199.
- [20] R.M. Batista, E.N.S. Muccillo, *Ceramics International* 37 (2011) 1929.
- [21] R.M. Batista, E.N.S. Muccillo, *Ceramics International* 37 (2011) 1047.
- [22] A.R. Hanifi, A. Torabi, T.H. Etsell, L. Yamarte, P. Sarkar, *Solid State Ionics* 192 (2011) 368.
- [23] A.R. Hanifi, A. Shinbine, T.H. Etsell, P. Sarkar, *Journal of Ceramic Processing Research* (2011) 336.
- [24] A.R. Hanifi, A. Shinbine, T.H. Etsell, P. Sarkar, *International Journal of Applied Ceramic Technology* 9 (2012) 1011.
- [25] A.R. Hanifi, M. Zazulak, T.H. Etsell, P. Sarkar, *Powder Technology* 231 (2012) 35.
- [26] A. Torabi, A.R. Hanifi, T.H. Etsell, P. Sarkar, *Journal of Electrochemical Society* 159 (2012) B201.
- [27] A.L. Vincent, A.R. Hanifi, J.-L. Luo, K.T. Chuang, A.R. Sanger, T.H. Etsell, P. Sarkar, *Journal of Power Sources* 215 (2012) 301.
- [28] A. Vincent, J.-L. Luo, K.T. Chuang, A.R. Sanger, *Journal of Power Sources* 195 (2010) 769.
- [29] L. Aguilar, S. Zha, Z. Cheng, J. Winnick, M. Liu, *Journal of Power Sources* 135 (2004) 17.